FORCED CONVECTION IN DRIVEN-LID SQUARE CAVITIES WITH IRREGULAR WALLS

Andressa Araújo Abreu
Department of Mechanical and Materials Engineering
Instituto Militar de Engenharia
22290-970 – Rio de Janeiro – RJ

Albino José Kalab Leiroz[♦]
Department of Mechanical Engineering – EE/COPPE
Universidade Federal do Rio de Janeiro
21945-970 – Rio de Janeiro – RJ

Abstract. *A numerical study of the momentum and energy transient transport processes within a square driven-lid cavity with an irregular wall is discussed in the present work. The transient velocity field behavior is analyzed in order to evaluate the basic physical phenomena associated with the forced convection phenomena and the influence of the irregular surface. A vorticity - stream function formulation is employed for the flow field analysis. The momentum and energy governing equations are discretized using the Finite-Difference Method. Initially, the irregular physical solution domain is transformed into a regular computational domain using numerical grid generation technique, allowing the clustering of points within solution high gradient regions and the control of grid line angles near the domain solid boundaries. The resulting system of algebraic equations is solved by an iterative method with local error control. Results are obtained for different shapes of the irregular surface, values of Reynolds and Prandtl showing the influence of these parameters on the velocity and temperature field evolution. Results show temperature and velocity profiles influenced by the combined effects of forced convection induced by the sliding-wall movement and by the irregular wall shape. Results also show the development of recirculation zones within the flow field and temperatures profiles influenced by the irregular surface.*

Keywords. *Convection-Diffusion, Numerical Methods, Driven-Lid Cavity, Irregular Wall.*

1. Introduction

The importance of studies on *momentum* and energy transport mechanisms within closed cavities is related to a wide variety of technological applications, which include the cooling of electronic equipments and coating of metallic surfaces. Besides the practical applications, confined cavity flows are used in basic physical phenomena studies since different flow aspects, such as vortices, secondary flow dynamics and hydrodynamic instabilities, can be observed in a yet simple geometry. Due to the different flow structures observed, cavity flows also provide test cases for performance evaluation of proposed numerical methodologies for fluid analysis.

Reviews of previews works on the flow structures and heat transfer processes inside closed cavities generated by the shear action of a moving wall (Shankar & Deshpande, 2000) or buoyancy (Kakaç et all, 1987) show the influence of several parameters on the transient evolution of the flow and temperature fields. The reviews also show the importance of numerical simulation for the flow field study since pure analytical solutions are limited to Stokes Flow regimes (Shankar & Deshpande, 2000). Numerical and phenomenological aspects are also discussed for tri-dimensional cavities stressing the limitations of two-dimensional analysis. Literature review on natural convection effects inside cavities with different geometries shows the influence of gravity on the flow field (Kakaç et all, 1987) and correlations for Nusselt number are also discussed for different conditions.

Natural convection effects in shallow and open two-dimensional cavities are numerically studied using a closed-cavity assumption and the Boussinesq approximation (Chan & Tien, 1985). The reduction of computational costs motivates the closed-cavity assumption. The flow field governing equations are written using a primitive variable approach and appropriate boundary conditions are applied to the approximated closed cavity. A SIMPLER based scheme is applied for the velocity-pressure coupling treatment. The agreement between numerical and experimental results, especially for low Rayleigh conditions, lends the closed-cavity assumption as appropriate.

Natural convection within rectangular shallow cavities is also studied considering diffusion along the horizontal surfaces (Wang & Daniels, 1994). A prescribed temperature difference between the vertical walls acts as the flow driving mechanism. Natural convection effects are studied for Prandtl of *0.05* and *0.733* and different values of Rayleigh. Results show that, for high Rayleigh conditions, nonlinearities become important and the flow departs from a diffusion controlled two-region structure.

Mixed convection effects in cubic cavities subjected to vertical temperature gradients are also numerically studied (Iwatsu & Hyun, 1995). The cavity upper wall slides at a constant velocity while kept at a higher temperature than the cavity lower wall and the cavity vertical walls are considered as insulated. Results are used to study the influence of the Richardson number on the flow field. Besides, comparison with planar results allows the evaluation of the limitations associated with two-dimensional models.

Hybrid techniques are also applied for the solution of the equations governing the flow field within two-dimensional cavities with a sliding wall (Pérez Guerrero & Cotta, 1992). A vorticity-stream function formulation is

---

[♦] Author to whom correspondence should be addressed. E-mail: leiroz@ufrj.br

applied. The partial differential equation for the stream function is integrated in one of the special variables, leading to an infinite system of ordinary differential equations, having a set of transformed stream functions are dependent variables. The transformed stream functions are appropriately defined from an eigenvalue problem. Once truncated to a sufficient large order, the system of ordinary differential is numerically solved leading to the transformed stream function distribution. The transformation is analytically inverted and the flow field determined within the cavity. For hybrid techniques, numerical approximations are limited to the solution of the ordinary differential equation system. Results are compared to pure numerical data, showing the convergence of the proposed expansion.

Experimental techniques are also applied for internal cavity flow and heat transfer analysis. Experiments used to capture the transient evolution of vortices within square, rectangular and semicircular driven cavities allow the determination of kinematical and topological data of the vorticity propagation (Migeon et al., 2000). A fixed and long surface is placed vertically and used as a solid cavity boundary while the remaining cavity walls are displaced leading to the internal cavity flow. Within the cavities used, boundary layer separation points, recirculation zone locations and sizes are determined. Experimental studies of flows inside cavities induced by differential wall temperatures indicate symmetry of the velocity and temperature field along the cavity mean plane (Ivey & Hamblin, 1989). Mixed convection within deep cavities is also studied using sliding walls and imposed temperature differences between the solid boundaries covering a broad range of Gr/Re^2 (Prassad & Koseff, 1996). Crystals are used for flow and temperature field visualization. Heat flux measurements are taken near the cavity bottom surface and results show that the Gr/Re^2 ratio has a weak effect on the heat transfer coefficient due to the local flow and heat transfer conditions.

In the present work, forced convection effects on the flow and temperature field evolution within square cavities with an irregular wall are discussed. Initially, a numerical procedure is applied to obtain a discretizing grid that allows the irregular domain treatment and the control of grid points. The flow governing equations, written using a vorticity-stream function formulation, and the energy conservation equation are discretized using the Finite Difference Method. The resulting system of algebraic equations is solved by an iterative procedure with local error control. Results for the transient evolution of the flow and temperature fields show the combined influence of the nondimensional transport parameters and the irregular surface profile.

2. Analysis

The solution domain is depicted in Fig.1, which also shows the system of coordinates employed in the current analysis. For the cavities considered in the present study, the upper wall slides at constant velocity U and the shape of the irregular bottom wall is described by an arbitrary function $F(x)$. The cavity solid boundaries are maintained at prescribed temperatures for the cases discussed in the present work.
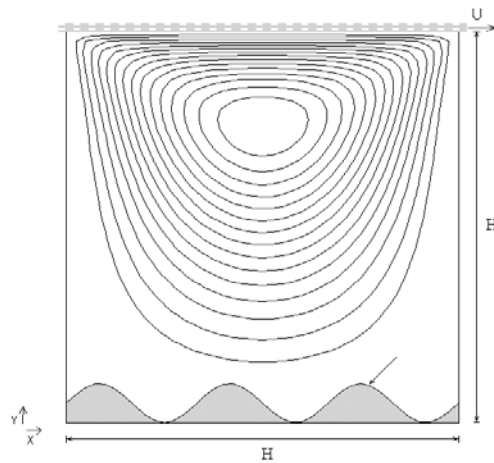
Figure 1. Solution domain, principal dimensions and Cartesian coordinate system.

Assuming constant thermo-physical properties and neglecting viscous dissipation effects the nondimensional governing equations for flow and temperature transient fields within the cavity are

$$\frac{\partial u_x}{\partial x} + \frac{\partial u_y}{\partial y} = 0 \tag{1}$$

$$\frac{\partial u_x}{\partial t} + u_x \frac{\partial u_x}{\partial x} + u_y \frac{\partial u_x}{\partial y} = -\frac{\partial P}{\partial x} + \frac{1}{Re}\left(\frac{\partial^2 u_x}{\partial x^2} + \frac{\partial^2 u_x}{\partial y^2}\right) \tag{2}$$

$$\frac{\partial u_y}{\partial t} + u_x \frac{\partial u_y}{\partial x} + u_y \frac{\partial u_y}{\partial y} = -\frac{\partial P}{\partial y} + \frac{1}{Re}\left(\frac{\partial^2 u_y}{\partial x^2} + \frac{\partial^2 u_y}{\partial y^2}\right) \tag{3}$$

$$\frac{\partial \theta}{\partial t} + u_x \frac{\partial \theta}{\partial x} + u_y \frac{\partial \theta}{\partial y} = \frac{1}{Re\,Pr}\left(\frac{\partial^2 \theta}{\partial x^2} + \frac{\partial^2 \theta}{\partial y^2}\right) \tag{4}$$

with boundary conditions

$$u_x = 1 \ , \ u_y = 0 \ , \ \theta = 0 \quad ; \quad y = 1 \ , \ 0 < x < 1 \tag{5}$$

$$u_x = 0 \ , \ u_y = 0 \ , \ \theta = 1 \quad ; \quad y = f(x) \ , \ 0 < x < 1 \tag{6}$$

$$u_x = 0 \ , \ u_y = 0 \ , \ \theta = 0 \quad ; \quad x = 0 \ , \ f(x) < y < 1 \tag{7}$$

$$u_x = 0 \ , \ u_y = 0 \ , \ \theta = 0 \quad ; \quad x = 1 \ , \ f(x) < y < 1 \tag{8}$$

and initial conditions

$$u_x = 0 \ , \ u_y = 0 \ , \ \theta = 0 \quad ; \quad 0 \le x \le 1 \ , \ f(x) \le y \le 1 \tag{9}$$

which correspond to stagnant and isothermal conditions.

The nondimensional variables in Eqs.(1-9) are defined as

$$x = \frac{x^*}{H}, \quad y = \frac{y^*}{H}, \quad u_x = \frac{u_x^*}{U}, \quad u_y = \frac{u_y^*}{U}, \quad t = \frac{t^*U}{H}, \quad P = \frac{P^*}{\rho U^2}, \quad \theta = \frac{T - T_o}{T_f - T_o} \tag{10}$$

using the cavity height (H) and the upper surface sliding velocity (U) as characteristic length and velocity, respectively. The nondimensional temperature is defined using the initial temperature T_o and the cavity bottom surface temperature T_f.

The Reynolds (Re) and Prandtl (Pr) numbers are defined as

$$Re = \frac{UH}{v}, \qquad Pr = \frac{v}{\alpha} \tag{11}$$

where v and α represent the kinematic viscosity and the thermal diffusivity, respectively.

In order to decouple the velocity and pressure fields and reduce the number of governing equations simultaneously solved, the primitive variable approach described in Eqs.(1-4) is rewritten in a vorticity-stream function formulation as

$$\frac{\partial \omega}{\partial t} + u_x \frac{\partial \omega}{\partial x} + u_y \frac{\partial \omega}{\partial y} = \frac{1}{Re}\left(\frac{\partial^2 \omega}{\partial x^2} + \frac{\partial^2 \omega}{\partial y^2}\right) \tag{12}$$

$$-\omega = \frac{\partial^2 \psi}{\partial x^2} + \frac{\partial^2 \psi}{\partial y^2} \tag{13}$$

with boundary conditions

$$\psi = 0 \quad ; \quad y = 1 \ , \ 0 < x < 1 \tag{14}$$

$$\psi = 0 \quad ; \quad y = f(x) \ , \ 0 < x < 1 \tag{15}$$

$$\psi = 0 \quad ; \quad x = 0 \ , \ f(x) < y < 1 \tag{16}$$

$$\psi = 0 \quad ; \quad x = 1 \ , \ f(x) < y < 1 \tag{17}$$

Initial stagnant conditions are written as

$$\psi = 0 \ , \ \omega = 0 \quad ; \quad 0 \le x \le 1 \ , \ 0 \le y \le 1 \tag{18}$$

Vorticity (ω) and Stream Function (ψ) are defined in terms of the velocity components, respectively, as

$$\omega = \frac{\partial u_y}{\partial x} - \frac{\partial u_x}{\partial y} \tag{19}$$

$$u_x = \frac{\partial \psi}{\partial y}, \quad u_y = -\frac{\partial \psi}{\partial x} \tag{20}$$

3. Numerical Aspects

The flow and temperature field governing equations are solved using the Finite-Difference Method (Anderson et all, 1984). Due to the nature of the physical phenomena involved, high gradients on the solution profiles are expected close to the cavity solid boundaries. Therefore, the numerical grid generation procedure allows the clustering of points and the control of grid angles near the cavity boundaries.

Initially the grid point distribution along the cavity boundaries is defined. Along the vertical walls, an algebraic equations (Anderson et all, 1984) expressed by

$$x = \xi \tag{21}$$

$$y = H \frac{(\beta + 2\alpha)\left[(\beta+1)/(\beta-1)\right]^{(\eta-\alpha)/(1-\alpha)} - \beta + 2\alpha}{(2\alpha+1)\left\{1 + \left[(\beta+1)/(\beta-1)\right]^{(\eta-\alpha)/(1-\alpha)}\right\}} \tag{22}$$
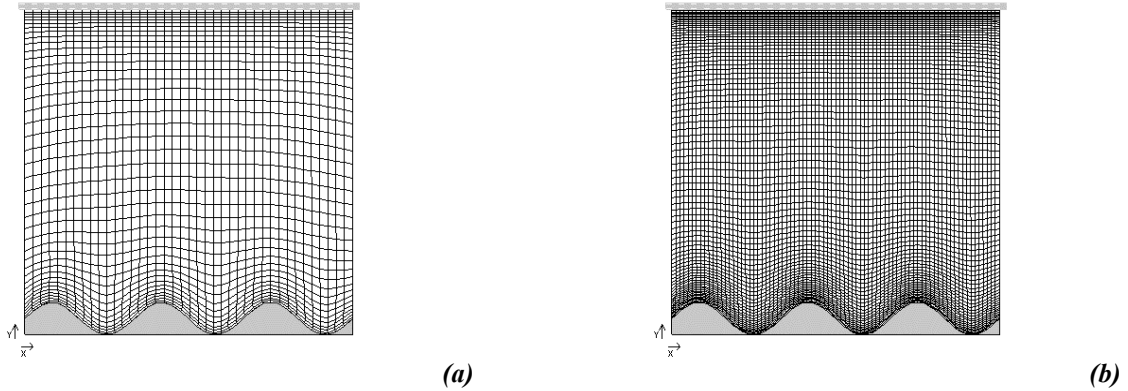
Figure 2: Discretizing grids within the physical domain for $f(x) = 0.5 \times (1.0 + sen(6\pi x))$ - *(a) 41x41* points and *(b) 81x81* points.

are applied allowing the clustering of points near the top and bottom walls. The parameters α and β allow the control of the clustering distribution and clustering intensity, respectively. Along the top and bottom cavity walls, an equidistant distribution of grid points is applied. For the interior points, the relation between physical (x,y) and transformed (ξ,η) variables is defined by elliptic partial differential equations describe by

$$\nabla^2 \xi = P(\xi,\eta) \tag{23}$$

$$\nabla^2 \eta = Q(\xi,\eta) \tag{24}$$

The numerical solutions of Eqs.(23-24) using the analytically established distribution along the cavity walls as boundary conditions, allows the determination of the metrics of the transformations. The source functions $P(\xi,\eta)$ and $Q(\xi,\eta)$ are used to control the grid angle and spacing near the solid boundaries. An iterative procedure is applied for the determination of $P(\xi,\eta)$ and $Q(\xi,\eta)$ from pre-determinate values of grid angle and spacing. Further details of the grid generation procedure are discussed in (Abreu and Leiroz, 2001). Grids obtained from the described procedure are shown in Fig.2 for different number of points and angle and spacing control applied to the top and bottom surface regions.

Using the transformation metrics, the governing equations are rewritten in terms of the transformed variables ξ and η and discretized using the BTCS scheme (Hoffman, 1992). The resulting system of algebraic equations is solved by an iterative method with local error control.

4.Results

Initially, the computational procedure was validated using limiting case of vanishing *Re* and regular bottom wall – *f(x) = 0* – which allows analytical solutions for the temperature field to be obtained. Deviations smaller than *2x10⁻⁴* between the analytical and numerical results are observed. Besides, the comparison with analytical results allows the calibration of the under-relaxation parameters associated with the iterative solution procedures. For the solution of the

algebraic systems resulting from the discretization procedures an under-relaxation parameters equal to *0.8* is used. An under-relaxation parameter equal to 0.6 is used for the evaluation of vorticity values along the solid boundaries. Calculations are performed until variations smaller than 10^{-3} are observed for the velocity and temperature fields.

(a)   (b)
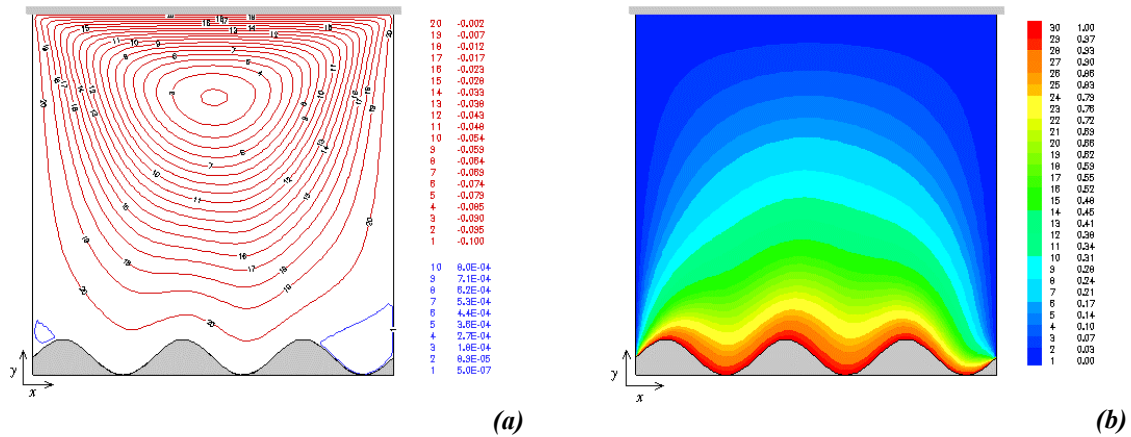
Figure 3. Steady state results for *(a)* stream function and *(b)* temperature fields for *Re = 1*, *Pr = 1* and $f(x) = 0.05 \times [1.0 + sen(6\pi x)]$.

Steady state stream function and temperature results for *Pr = 1* $f(x) = 0.05 \times [1.0 + sen(6\pi x)]$ and *Re = 1, 100* and *1000* are shown in Figs. (3-5). For low Reynolds (*Re = 1*), stream function and temperature profiles, shown in Fig.3, have a symmetrical behavior near the top cavity surface. Within the irregular-wall near region, the solution profiles become distorted. It is worth mentioning that for a profile with *10%* of the cavity height, results show irregular wall effects near the cavity medium plane (*y = 0.5*). For *Re = 100*, a displacement of the primary recirculation center parallel to the top surface moving direction is observed when results depicted on Figs. 3a and 4a are compared. Besides, results also show secondary recirculation zones near the irregular surface of similar size and strength for *Re = 1* and *100*. The *Re* increase also distorts the temperatures fields inside the cavity as shown in Figs.3b and 4b. The upward fluid movement is associated with a pronounced irregular surface temperature effect and smoother gradients near *x = 0*, as depicted in Fig.4b. Results for *Re = 1000* are depicted in Fig.5 showing an increase in size and intensity of the secondary recirculation zones. The primary recirculation zone center is displaced towards the cavity center as a result of the interaction with the enlarged secondary recirculation zones. Convective effects on the temperature field become more pronounced as shown in Fig.5 with secondary recirculation zones associated with smoother temperature gradients.

(a)   (b)
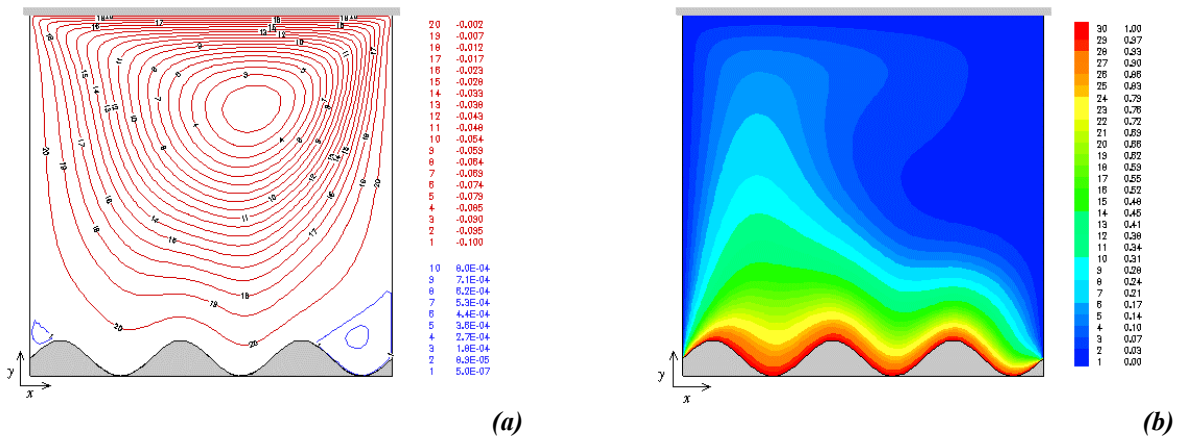
Figure 4. Steady state results for *(a)* stream function and *(b)* temperature fields for *Re = 100*, *Pr = 1* and $f(x) = 0.05 \times [1.0 + sen(6\pi x)]$.

Comparing results in Figs.3b, 5b and 6 allows the evaluation of the Prandtl number (*Pr*) influence on the temperature profiles. When compared with Fig. 3b, results in Fig. 6a indicate more intense convective effects resulting on a nonsymmetrical temperature field. Stepper temperature gradients are observed along the vertical wall at *x = 0* for *Re = 1* and *Pr = 10* (Fig. 6a). Near the *x = 1* wall, a thermal boundary layer broadening is also observed in Fig. 6a due the downward fluid movement. It is noteworthy the appearance of a high temperature region associated with the secondary recirculation zone associated with the downward fluid motion near *x = 1* for *Re = 1000* as shown in Fig. 6b. The increase of *Pr* enhances convective effects within the secondary recirculation zones for which diffusion is dominant in low Peclet number situations.

(a)

(b)
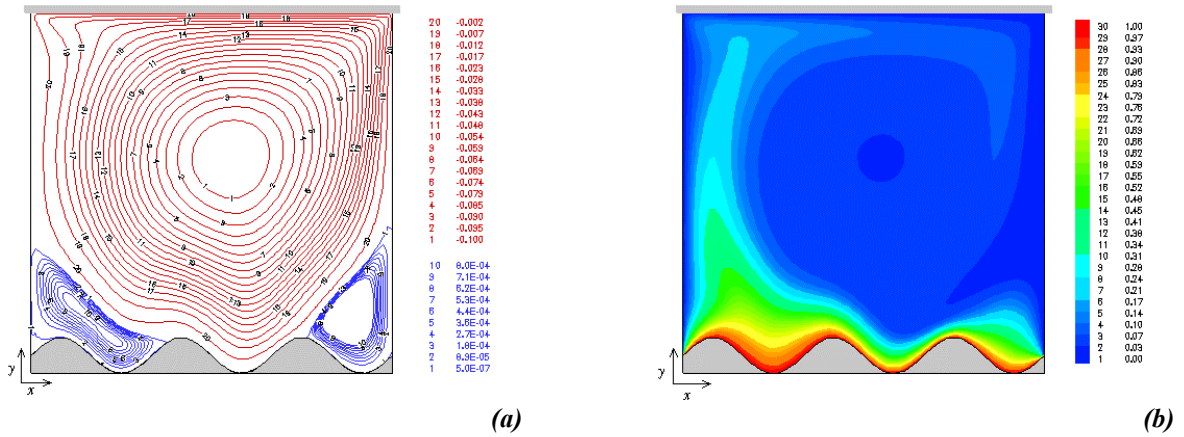
Figure 5. Steady state results for *(a)* stream function and *(b)* temperature fields for *Re = 1000*, *Pr = 1* and $f(x) = = 0.05 \times [1.0 + sen(6\pi x)]$.

(a)

(b)
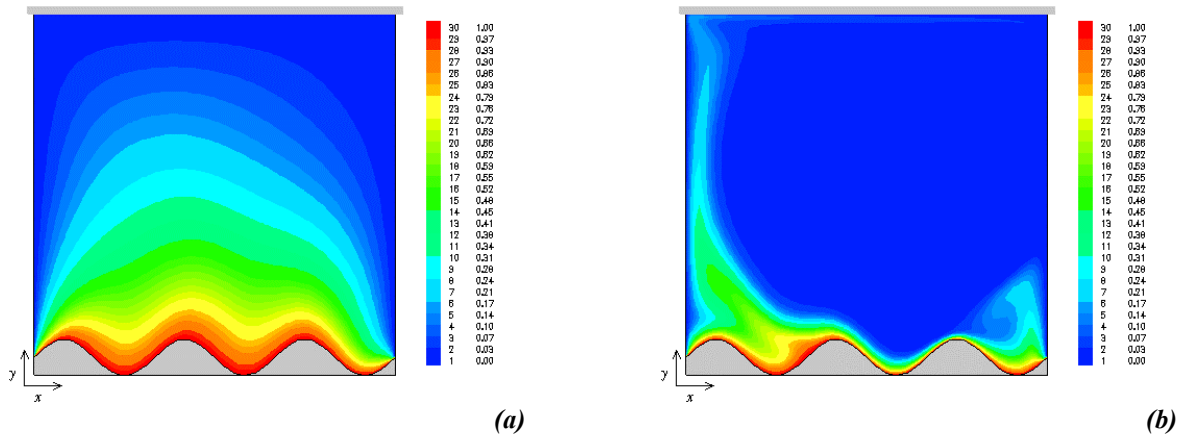
Figure 6. Steady state results for temperature fields for *(a)* *Re = 1*, *Pr = 10* and *(b)* *Re = 1000*, *Pr = 10* - $f(x) = = 0.05 \times [1.0 + sen(6\pi x)]$.

(a)

(b)
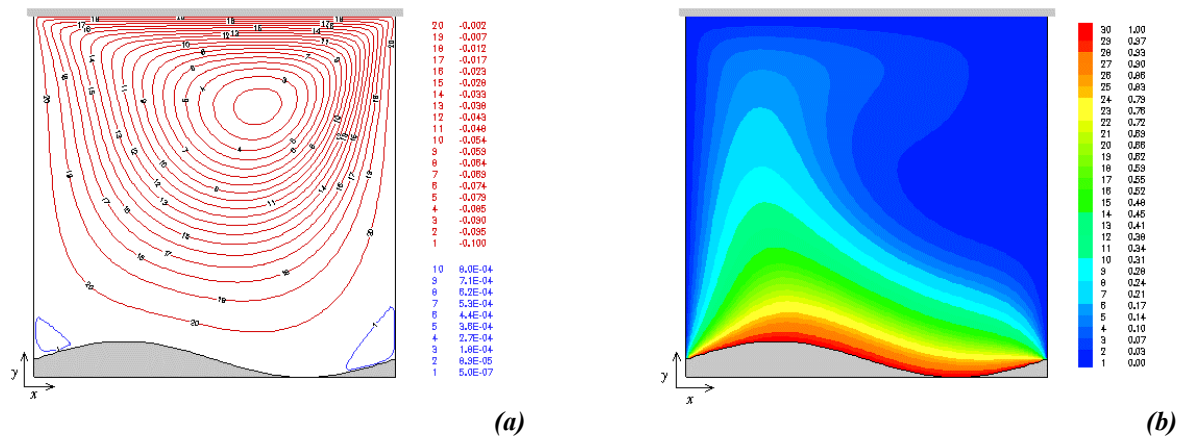
Figure 7. Steady state results for *(a)* stream function and *(b)* temperature fields for *Re = 100*, *Pr = 1* and $f(x) = = 0.05 \times [1.0 + sen(2\pi x)]$.

(a)   (b)
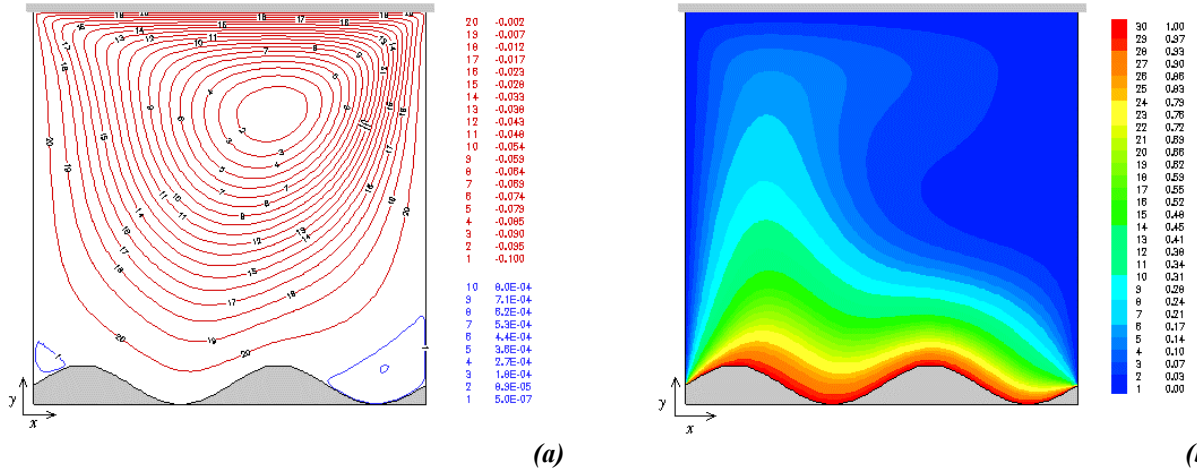
Figure 8. Steady state results for *(a)* stream function and *(b)* temperature fields for *Re = 100, Pr = 1* and *f(x) =*
$= 0.05 \times [1.0 + sen(4\pi x)]$.

Stream function and temperature distributions are shown in Fig. 7 and 8 for different irregular surface shapes. Results show that, for the parameters used in the simulations, the irregular surface influence is restricted to the lower cavity region with similar velocity and temperature profiles near to sliding surface. Besides, stream function results show that as the frequency of the harmonic function used to describe the lower surface is increased (Fig. 8a), the secondary flow near the edges is intensified. For the cases studied, no significant interaction between the primary and secondary flows is observed.

(a)   (b)

(c)   (d)
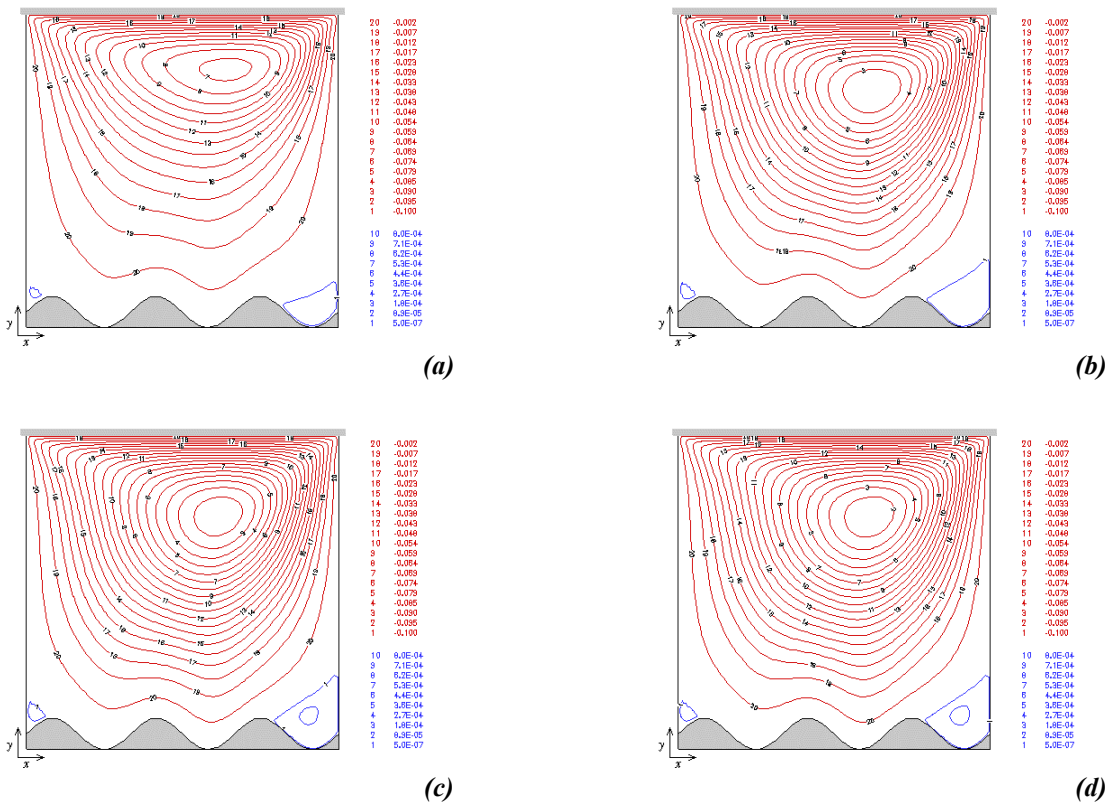
Figure 9. Transient stream function results for *(a)* t = 1.0, *(b)* t = 4.0, *(c)* t = 8.0 and *(d)* t = 12 - Re = 100, Pr = 1 and
$f(x) = 0.05 \times [1.0 + sen(6\pi x)]$.

The transient evolution of the stream function and temperature fields are shown for *Re = 100* and *Pr = 1* in Figs. 9 and 10 respectively. Results depicted in Fig.9 show irregular surface influence on the flow field for even for initial times (Fig.9a). The development of primary and secondary recirculation zones is also depicted in Fig.9. The development of the recirculation zones results in the displacement of the primary recirculation center towards to cavity mid-plane and the growth of the secondary recirculation near the cavity lower edges. The temperature field development (Fig.10) is

diffusion-controlled for initial times as the developing flow field limits convective effects. Diffusion remains important as the temperature field develops within the irregular wall near region due to the low velocities associated. As velocity and temperature fields develop, the influence of upward and downward fluid movement become important near the $x = 0$ and $x = 1$, respectively. Hydrodynamic steady-state conditions are reached prior to the full development of the temperature field, which occurs at $t = 17.7$.

Transient flow field and temperature results for $Re = 1000$ are shown in Figs. 11 and 12, respectively. Steady-state conditions for the solution fields are reached for $t = 65.7$ for $Re = 1000$. The flow field development is initiated with high velocity gradients near the sliding surface and no significant secondary recirculation zones, as shown in Fig. 11a. During the development of the primary recirculation zone, the velocity gradients become smoother near the moving boundary and the irregular surface influence becomes significant as depicted in Figs. 11b-11d. The secondary recirculation zone develops along the lower cavity edges showing an increase in both size and strength. It should be mentioned that a secondary recirculation zones also develops along the $x = 1$ wall from boundary layer separation (Fig. 11b). The vertical wall and lower edge recirculation zones at $x = 1$ coalescence into a single zone shown on Fig. 11d – 11e. Secondary flow evolution influences the temperature gradient behavior near the irregular wall as shown in Fig.12. The recirculation zones are associated with weaker convective effects and smother temperature gradients
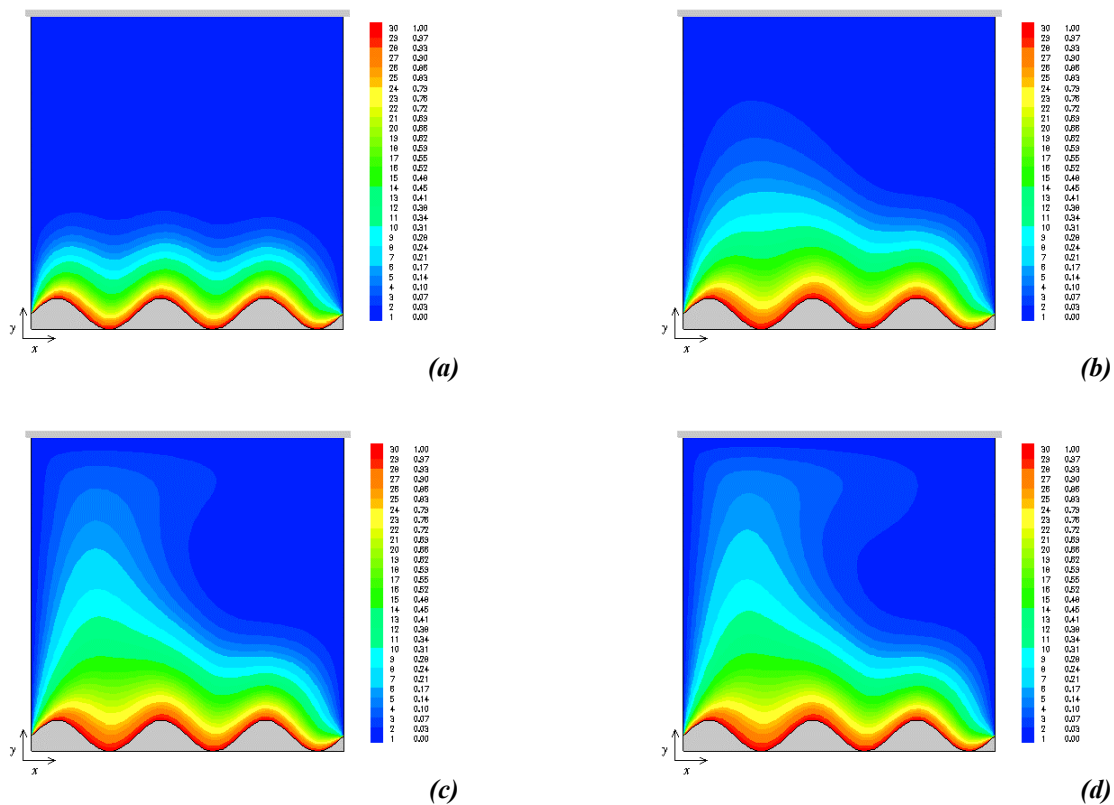
Figure 10. Transient temperature field results for *(a)* $t = 1.0$, *(b)* $t = 4.0$, *(c)* $t = 8.0$ and *(d)* $t = 12$ - $Re = 100$, $Pr = 1$ and $f(x) = 0.05 \times [1.0 + sen(6\pi x)]$.

5.Conclusions

The present work revisits the problem of transport of *momentum* and energy inside a driven-lid cavity modified by the introduction of an irregular wall of sinusoidal shape in order to enhance the different phenomenological mechanics displayed by the classic formulation. Results show that, for the parameters used in the simulations, a smooth transition between the profiles obtained considering regular and irregular surfaces can be expected. Besides, irregular surface can be used to enhance secondary flows on the cavity lower edges and that interaction between primary and secondary flows is present. Further studies are necessary in order to quantify the irregular surface effects on the *momentum* and heat transfer coefficients along the cavity boundaries.

6.Acknowledgement
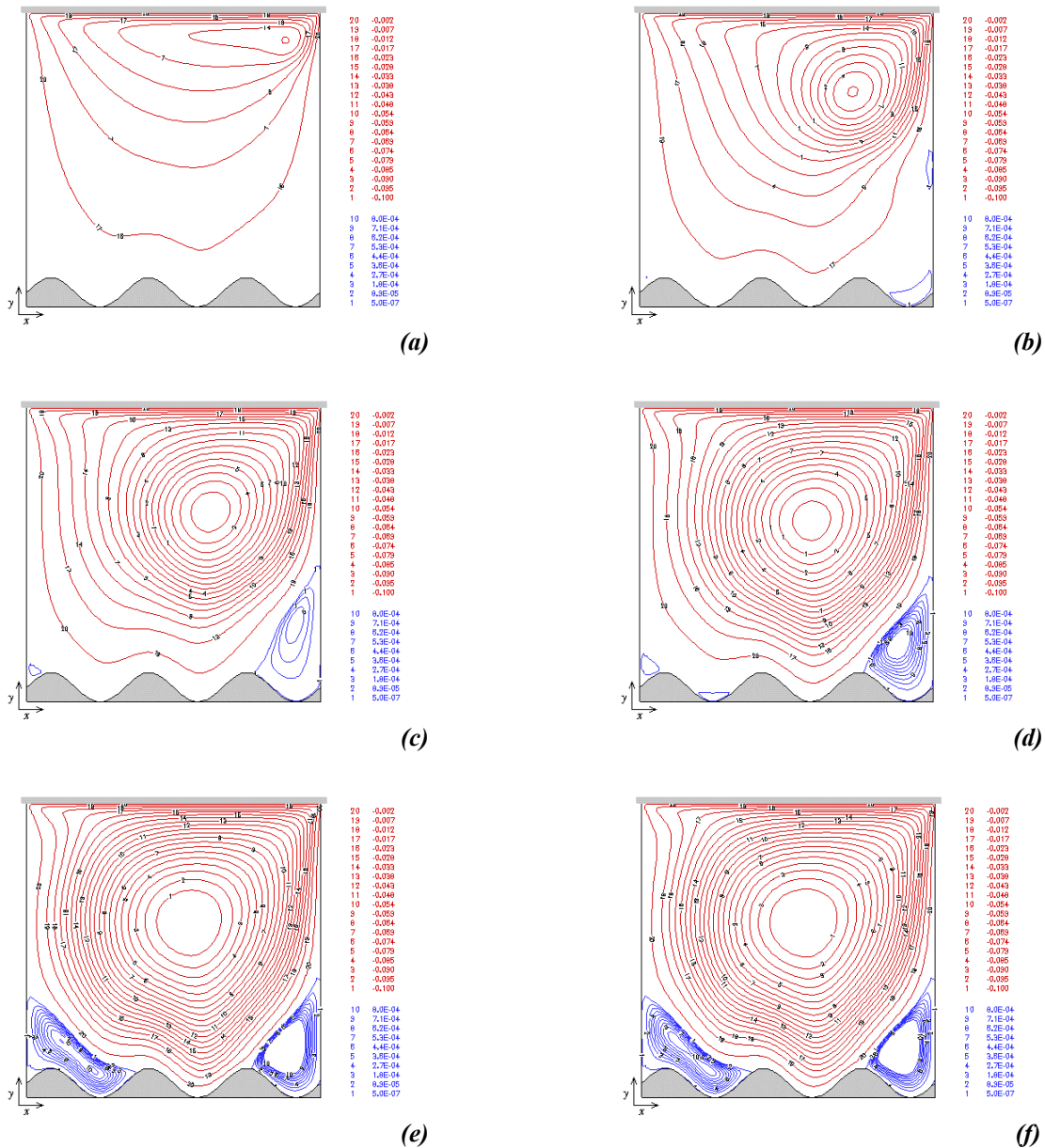
Figure 11. Transient stream function results for *(a) t = 1.0*, *(b) t = 4.0*, *(c) t = 8.0*, *(d) t = 12*, *(e) t = 30* and *(f) t = 45* - *Re = 1000*, *Pr = 1* and $f(x) = 0.05 \times [1.0 + sen(6\pi x)]$.

7. References

Abreu, A.A., Leiroz,A.J.K., 2001, "A Numerically Generated Grid for Irregular Wall Cavity Analysis", Proceedings of the 16th Brazilian Congress of Mechanical Engineering, Uberlândia, Brazil, pp. 557-566, *in Portuguese.*

Anderson, D. A., Tannehill, J. C. and Pletcher, Richard H., 1984, "Computational Fluid Mechanics and Heat Transfer", Hemisphere Publishing Corporation, New York, USA.

Chan, Y.L. and Tien, C.L., 1985, "A Numerical Study Of Two-dimensional Laminar Natural Convection in Shallow Open Cavities", Int. Journal of Heat and Mass Transfer, Vol.28, pp. 603-612.

Hoffman, J. , 1992, "Numerical Methods for Engineers and Scientists, McGraw-Hill, New York, USA.

Ivey, G.N. and Hamblin, P.F., 1989, "Convection Near the Temperature of Maximum Density for High Rayleigh Number, Low Aspect Ratio, Rectangular Cavities", Journal of Heat Transfer, Vol.111, pp. 100-105.

Iwatsu, R. and Hyun, J.M., 1995, "Three-Dimensional Driven-Cavity Flows with a Vertical Temperature Gradient", Int. Journal of Heat and Mass Transfer, Vol.38, pp. 3319-3328.

Kakaç, S., Shah, R.K. and Aung, W., 1987, "Handbook of Single Phase Convective Heat Transfer", John Wiley, New York, USA.

Migeon, C., Texier, A. and Pineau, G., 2000, "Effects of Lid-Driven Cavity Shape on the Flow Establishment Phase", Journal of Fluids and Structures, Vol.14, pp. 469-488.

Perez Guerrero, J.S. and Cotta, R.M., 1992, "Integral Transform Solution for the Lid-Driven Cavity Flow Problem in Streamfunction – Only Formulation", Int. Journal for Numerical Methods in Fluids, Vol.15, pp. 399-409.

Prasad, A.K. and Koseff, J.R., 1996, "Combined Forced and Natural Convection Heat Transfer in a Deep Lid-Driven Cavity Flow", Int. Journal of Heat and Fluid Flow, Vol.17, pp. 460-467.

Shankar, P.N. and Deshpande, M.D., 2000, "Fluid Mechanics in Driven Cavity", Annual Review in Fluid Mechanics, Vol. 32, pp. 93-136.

Wang, P. and Daniels, P.G., 1994, "Numerical Study of Thermal Convection in Shallow Cavities with Conducting Boundaries", Int. Journal of Heat and Mass Transfer, Vol.37, pp. 387-399.
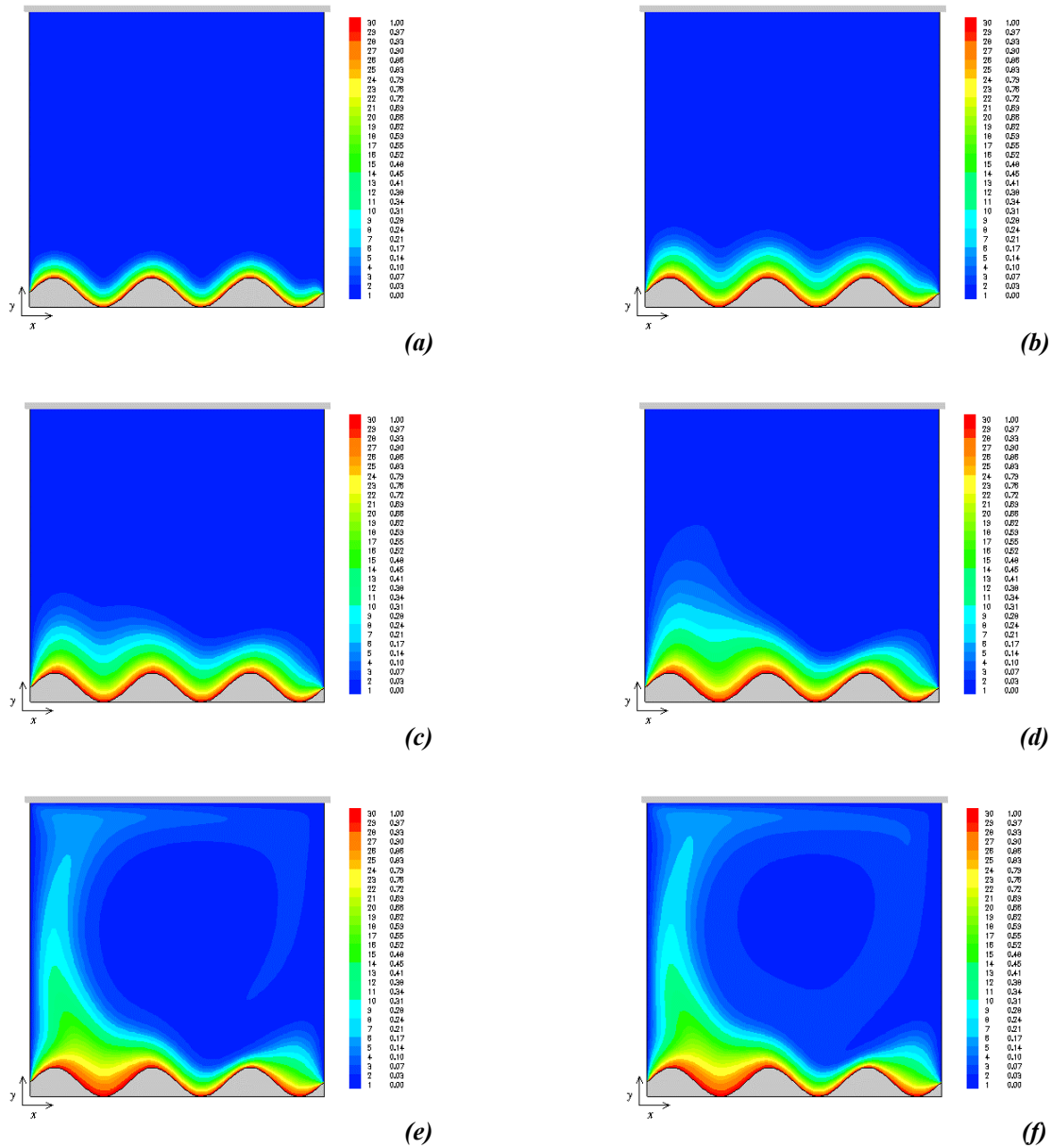
Figure 12. Transient temperature field results for *(a)* *t = 1.0*, *(b)* *t = 4.0*, *(c)* *t = 8.0* and *(d)* *t = 12 - Re = 100, Pr = 1* and $f(x) = 0.05 \times [1.0 + sen(6\pi x)]$.